Journal of Alloys and Compounds 509 (2011) 9322–9328

Contents lists available at ScienceDirect

Journal of Alloys and Compounds

journal homepage: www.elsevier.com/locate/jallcom

V–Ni–Ti multi-phase alloy membranes for hydrogen purification

G. Song[a], M.D. Dolan[b,*], M.E. Kellam[a], D. Liang[a], S. Zambelli[b]

[a] CSIRO Process Science and Engineering, Clayton, VIC 3168, Australia
[b] CSIRO Energy Technology, 1 Technology Court, Pullenvale, QLD 4069, Australia

ARTICLE INFO

Article history:
Received 11 May 2011
Received in revised form 8 July 2011
Accepted 8 July 2011
Available online 2 August 2011

Keywords:
Hydrogen
Membrane
Alloy
Vanadium
Nickel
Titanium
Body-centred cubic

ABSTRACT

Hydrogen-selective membranes formed from body centred cubic alloys can exhibit very high hydrogen permeability, but are prone to brittle failure due to excessive hydrogen absorption. Until issues associated with this are overcome, these materials will not provide a viable alternative to Pd-based membranes. Multi-phase V–Ni–Ti alloys which contain a significant proportion of a BCC component show promise for this application. In order to examine this system in greater detail, alloys of the general form $V_{85-x}Ti_xNi_{15}$, in which x was varied between 0 and 30 (at.%), were fabricated via arc melting and electrical-discharge wire cutting. Hydrogen permeation measurements of Pd-coated samples at 400 °C showed a monotonic increase in permeability with increasing Ti, reaching a maximum of 1.0×10^{-7} mol H_2 m^{-1} s^{-1} $Pa^{-0.5}$ for the $V_{55}Ti_{30}Ni_{15}$ alloy at 400 °C. The driving force for hydrogen transport is provided by hydrogen absorption, which varies non-linearly with Ti content, and is dependent on the volume fraction of BCC phase, and levels of Ti and Ni solution in the BCC phase. Diffusion coefficients of atomic H through the bulk alloys alloys are dependent largely on microstructure. Whereas the $V_{85}Ni_{15}$ alloy forms a single phase microstructure, progressive substitution of V with Ti introduced several minor phases; a NiTi-type phase (formed when $x \geq 5$), and a $NiTi_2$-type phase (formed when $x \geq 10$), both as V-containing solid solutions. These minor phases act as barriers to hydrogen diffusion, resulting in a significantly reduced diffusion coefficient compared to single-phase BCC alloys. Importantly, the mechanical stability of these alloys appears to be enhanced by the multi-phase microstructure. These alloys therefore show great promise for meeting future flux, cost and durability targets.

1. Introduction

Gas separation membranes offer several potential advantages over PSA/TSA-type hydrogen purification systems, including continuous separation, higher operating temperatures and the potential for process intensification through integration with gas conversion reactions (*e.g.*, water gas shift and steam methane reforming). Membrane technology still lags behind solvent and sorbent technology for hydrogen-related applications, however, and is currently restricted to niche applications such as bench-top hydrogen purification and several industrial trials. Uptake of membrane technology for H_2/CO_2 separation on a large scale will not occur until significant improvements in hydrogen flux, durability and cost have been achieved.

Of the main classes of hydrogen-selective (alloy, dense ceramic, microporous inorganic, polymer) membranes, alloy membranes offer several favourable characteristics for fossil fuel-based hydrogen production, namely an intrinsically pure hydrogen product, stability in syngas environments and temperatures of operation compatible with hydrocarbon conversion reactions. Aside from palladium alloys, body-centred cubic (BCC) metals are one of the most promising classes of alloy membrane. The hydrogen permeabilities of pure BCC metals such as V, Ta and Nb at 400 °C are all in excess of 1×10^{-7} mol m^{-1} s^{-1} $Pa^{-0.5}$, an order of magnitude greater than Pd [1].

The high permeability of BCC metals can be attributed to high solubility of hydrogen and fast hydrogen diffusion [2]. The high levels of hydrogen absorption, however, can degrade the mechanical properties of these alloys to the point where they suffer from brittle failure under the typical operating conditions (temperatures around 400 °C, hydrogen partial pressures less than 10 bar).

Several groups have attempted to abate the effects of brittle failure of these metals by forming alloys with reduced hydrogen absorption. Vanadium has received most attention because of its ability to maintain the BCC structure over a wider compositional range than Ta or Nb. The best known BCC alloys for membrane applications are vanadium-based solid solutions containing Ni [3–6], and Al, Ag, Pd, Fe, Mn, Co and Cu [7–11].

Multi-phase, BCC-based alloys have also been explored. Formation of NiTi and $NiTi_2$ phases within a BCC matrix has been observed in V–Ni–Ti [12,13], Nb–Ti–Ni [14,15] and Ta–Ti–Ni alloy membranes [13], along with analogous phases in Nb–Ti–Co

---

* Corresponding author. Tel.: +61 7 3327 4126.
E-mail address: michael.dolan@csiro.au (M.D. Dolan).

0925-8388/$ – see front matter © 2011 Elsevier B.V. All rights reserved.
doi:10.1016/j.jallcom.2011.07.020

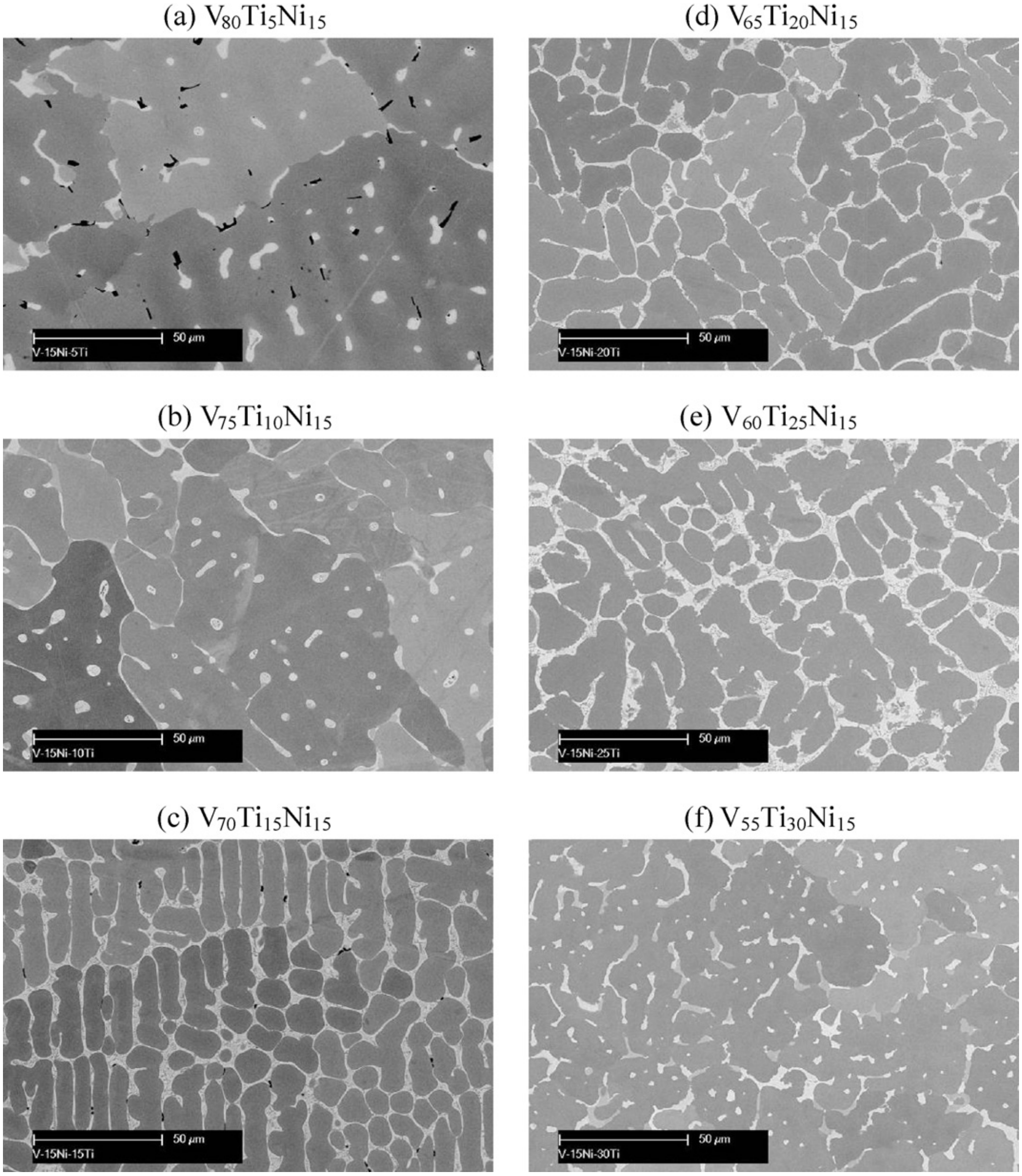

Fig. 1. Electron micrographs (BSE mode) of (a) $V_{80}Ti_5Ni_{15}$, (b) $V_{75}Ti_{10}Ni_{15}$, (c) $V_{70}Ti_{15}Ni_{15}$, (d) $V_{65}Ti_{20}Ni_{15}$, (e) $V_{60}Ti_{25}Ni_{15}$ and (f) $V_{55}Ti_{30}Ni_{15}$. Each image shows an area of 190 μm × 140 μm. The black features are pores.

[16] and Nb–Zr–Ni alloys [17]. In each case, the Ni-based compounds are purported to stabilise the alloy membranes against embrittlement. Of these examples, the $Nb_{40}Zr_{30}Ni_{30}$ alloy with 40% of the BCC solid solution exhibited the highest permeability (4.6×10^{-8} mol m^{-1} s^{-1} Pa$^{-0.5}$ at 400 °C), however significant increases in permeability are required to meet future performance targets. NiTi is best known as a shape-memory alloy with high mechanical strength and high ductility [18,19], but is also of interest for hydrogen storage applications. When hydrided, NiTi forms an interstitial solid solution [20] with H preferentially occupying the octahedral interstice. According to Schmidt et al. [21] and Wipf [22], the diffusion coefficient of hydrogen in α-NiTi hydride at 400 °C ($\sim 2 \times 10^{-10}$ m^2 s^{-1}) is around two orders of magnitude lower than in V ($\sim 2 \times 10^{-8}$ m^2 s^{-1}). Similarly, the hydrogen absorption of NiTi is significantly less than V. Using the numerical expression presented by Schmidt et al., the H/M ratio of NiTi at 400 °C and 6 bar is ∼0.06, compared to ∼0.58 for V [2]. This reduced diffusion coefficient and driving force suggest that formation of NiTi within a V-based BCC alloy would decrease the hydrogen permeation rate significantly. This was confirmed by Hashi et al. [14], who measured the permeability of NiTi to be 3 orders of magnitude lower than V.

The $V_{85}Ni_{10}Ti_5$ alloy reported by the present authors [8] demonstrated the positive effect that Ti can have on hydrogen permeability when added in certain proportions, with the permeability of $V_{85}Ni_{10}Ti_5$ being ∼4 times greater than $V_{85}Ni_{15}$ at 400 °C, and up to 8 times greater than V–Ni–Ti alloys reported previously. The main reason for this high permeability was found to be due to a large increase in hydrogen absorption, which was countered slightly by a small decrease in the hydrogen diffusion coefficient. This observed behaviour may be due to elemental partitioning within the multi-phase microstructure: the addition of Ti to the V–Ni solid solution precipitates several NiTi-rich compounds, thereby depleting Ni from the solid solution and enriching the V content of the primary BCC phase. This in

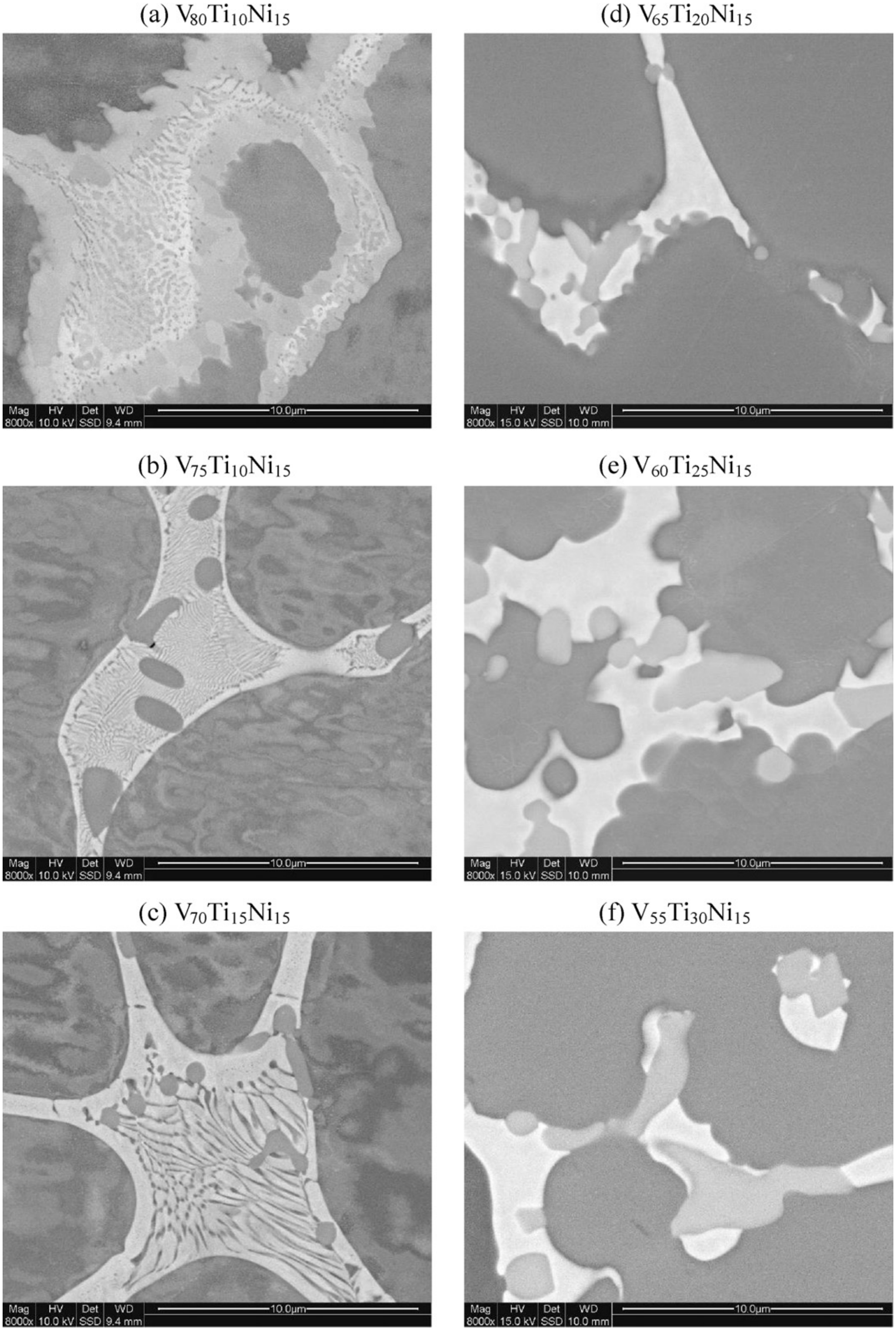
(a) $V_{80}Ti_{10}Ni_{15}$ (d) $V_{65}Ti_{20}Ni_{15}$

(b) $V_{75}Ti_{10}Ni_{15}$ (e) $V_{60}Ti_{25}Ni_{15}$

(c) $V_{70}Ti_{15}Ni_{15}$ (f) $V_{55}Ti_{30}Ni_{15}$

Fig. 2. Electron micrographs (BSE mode) of (a) $V_{80}Ti_5Ni_{15}$, (b) $V_{75}Ti_{10}Ni_{15}$, (c) $V_{70}Ti_{15}Ni_{15}$, (d) $V_{65}Ti_{20}Ni_{15}$, (e) $V_{60}Ti_{25}Ni_{15}$ and (f) $V_{55}Ti_{30}Ni_{15}$. Each image shows an area of $16\,\mu m \times 14\,\mu m$.

turn increases the absorption of hydrogen by the primary phase, and increases the hydrogen permeability of the alloy.

The aim of the present work is to further explore the V–Ni–Ti system illustrate the effect of further Ti additions, up to and beyond Ti:Ni molar equivalency. An alloy series has been devised, therefore, with the general formula $V_{85-x}Ti_xNi_{15}$, where x varies from 0 to 30 at.%. Hydrogen permeability, solubility and diffusion coefficients will be evaluated, and compared against microstructural properties such as phase compositions, crystal structures, lattice parameters, and volume fractions.

2. Methods

2.1. Membrane preparation

High purity (99.9%) vanadium, titanium and nickel pellets were melted several times until homogeneous on a water-cooled copper hearth using a vacuum/argon arc melter. The arc-melted ingots were sectioned using electrical discharge machining (EDM), and the surfaces were polished, chemically cleaned and RF-sputtered with 500 nm of Pd to promote H_2 dissociation. Each disk was approximately 800 μm thick.

2.2. Microstructural analysis

The pre-permeation alloy microstructure was examined in back-scattered electron (BSE) mode a Quanta 400 FEG-SEM equipped with X-ray energy dispersive spectroscopy (EDS). Surfaces were polished using diamond paste prior to analysis.

XRD measurements were made with a Bruker D8 advance X-ray diffractometer employing Cu Kα radiation with a tube voltage of 40 kV and current of 40 mA. The sample was scanned over the 2-theta range 20–120° with a step size of 0.02° and a count time of 4 s. Analyses were performed on the collected X-ray diffraction (XRD) data using the Bruker XRD search match program EVA. Crystalline phases were identified from the ICDD-JCPDS powder diffraction database.

Electron back-scatter diffraction (EBSD) was used to confirm the presence of several phases present at low concentrations. A JEOL 7001F field emission gun scanning electron microscope (FEG-SEM) was used to collect Kikuchi patterns under specimen inclination of 70° and operating at 20 kV. The acquired EBSD patterns were indexed for phase determination using Oxford Instruments Channel 5 HKL software.

Quantitative composition analysis was performed on the BCC matrix and secondary-phase compounds using a JEOL 8500F electron microprobe. The intensity measurements were conducted at 12 kV accelerating voltage and a beam current of 30 nA.

2.3. Permeation testing

Hydrogen permeability was measured using the constant pressure method at 400 °C. Membranes were sealed in a custom inconel module using annealed copper gaskets with an internal diameter of 1.60 cm, giving an active area of 2.01 cm^2. Testing conditions were selected correspond with the US Department of Energy membrane testing protocol [23]. During permeation testing, the feed-side was supplied with a 90% H_2 + 10% CO_2 mix. at 200 ml/min at a pressure of 6.0 bar(a). An argon stream was passed over the low-pressure surface at 200 mL min^{-1}. The hydrogen content in the Ar stream was measured using a gas chromatograph, and from this value hydrogen flux was calculated. The integrity of the membrane was confirmed by the absence of CO_2 in the permeate stream. Permeability was calculated as the gradient of hydrogen flux against ($P_1^{0.5} - P_2^{0.5}$), where P_1 is the feed-side pressure and P_2 is the permeate-side pressure.

2.4. Hydrogen absorption measurements

The hydrogen uptake of each alloy with varying hydrogen pressure and temperature was measured using the Sieverts' method. Pd-coated samples of each alloy were used for the testing, and given the difference in total Pd thickness (1 μm) compared to the V-based alloy (~800 μm), the contribution of the Pd to each solubility isotherm was negligible. Measurements were performed at 400 °C between 0 and 20 bar(a) in a custom stainless steel chamber with VCR-type face sealing. Hydrogen (99.999%) was supplied to the apparatus from a storage cylinder.

3. Results

3.1. Microstructure

A previous publication from this group reported on the single-phase BCC microstructure of the $V_{85}Ni_{15}$ alloy [4]. Partial substitution of V by Ti, however, can result in a multi-phase microstructure. BSE-SEM images of the cast alloys containing Ti are shown in Fig. 1. These alloys have typical dendritic solidification microstructures with different amounts of minor phases formed in the interdendritic regions. For the $V_{80}Ti_5Ni_{15}$ alloy, isolated pockets of these minor phases are distributed between dendrites or dendrite arms which have coalesced because of the high volume fraction of V-matrix solution. With increasing Ti content, the minor phases located in the interdendritic regions become continuous, preventing the dendrite arms from bridging. The implications on the tortuosity of the BCC pathway for hydrogen diffusion will be discussed in Section 3.4.

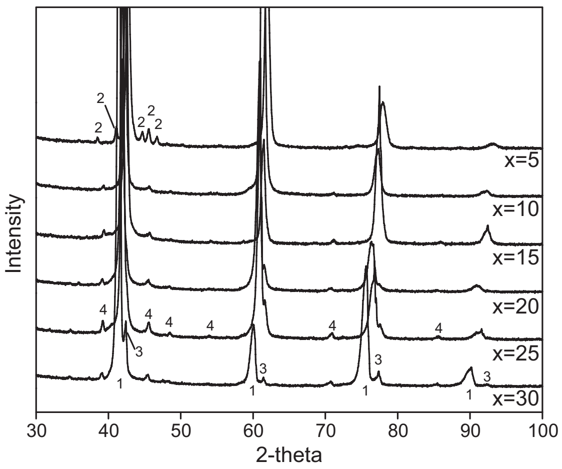

Fig. 3. X-ray diffraction patterns for $V_{85-x}Ti_xNi_{15}$ alloys. Peaks corresponding to V (1), V_2Ni (2), NiTi (3) and $NiTi_2$ (4) are labelled.

Three phases are present in each of the as-solidified $V_{85-x}Ni_{15}Ti_x$ alloys: the dendritic BCC matrix, and two interdendritic phases, all of which are clearly illustrated in the higher magnification images shown in Fig. 2. In the $V_{80}Ti_5Ni_{15}$ alloy, the interdendritic $V_{62.9}Ti_{8.7}Ni_{28.4}$ phase is analogous to the V_2Ni compound (with partial substitution of Ti for V). The presence of the V_2Ni compound was confirmed by XRD (Fig. 3). The third (brightest) phase in the $V_{80}Ti_5Ni_{15}$ alloy was below the XRD detection limit, but EBSD analysis identified this as a cP2 NiTi-type structure.

For $5 \leq x \leq 30$ alloys, the bright interdendritic phase shown in Fig. 2 is a NiTi-based compound with varying amounts of dissolved V. Another Ti-rich compound with an approximate composition $(Ti,V)_{\sim 70}Ni_{\sim 30}$ is embedded within the interdendritic region, and the composition of this phase is very close to that of $NiTi_2$. XRD patterns (Fig. 3) confirm the presence of the BCC matrix and $NiTi_2$ in all alloys, and NiTi for $x \geq 20$ alloys (in which the peak shift of the BCC matrix to lower angles allows these NiTi peaks to become visible).

Details of the microstructural characterisation of each alloy in the $V_{85-x}Ti_xNi_{15}$ series, including phases present, atomic compositions, lattice parameters and volume fractions of each phase, are shown in Table 1. The low concentrations of minor phases (*i.e.*, those with space groups 136, 221 or 227) prevented accurate lattice parameter measurements from being obtained. Lattice parameters in Table 1 corresponding to these phases are taken from literature values of V_2Ni [24], NiTi and $NiTi_2$ [25] respectively.

The microstructural features of the V-rich BCC matrix depend on the specific alloying addition. In the case of these V–Ni–Ti alloys, Ti dissolves into the solid solution which lowers the solubility of Ni. This leads to partitioning of Ni and Ti, resulting in the formation of interdendritic phases such as NiTi and $NiTi_2$. Conversely, the combined presence of Ti and Ni in the solid solution expands the lattice linearly with increasing bulk Ti content (see Table 1). This is expected when considering the atomic radii of Ti (0.1462 nm), V (0.1316 nm) and Ni (0.1246 nm) [26], and the increase in the relative proportion of Ti and Ni retained in the matrix. In addition, the combined presence of Ti and Ni in the solid solution is likely to cause strain in the lattice, as supported by the V-matrix peak broadening shown in Fig. 3.

3.2. Hydrogen absorption

Fig. 4 shows hydrogen absorption isotherms at 400 °C for all alloys in the series expressed in terms of hydrogen to metal ratio,

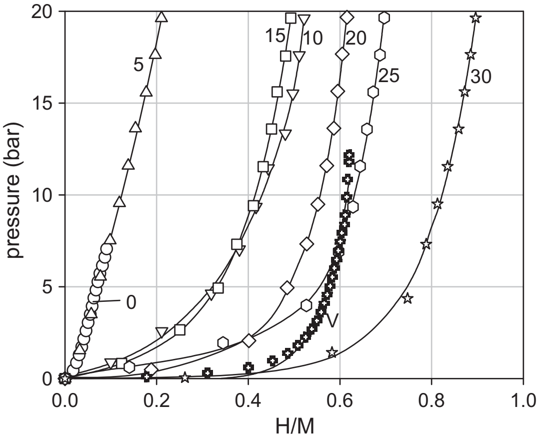

Fig. 4. Hydrogen absorption isotherms for $V_{85-x}Ti_xNi_{15}$ alloys and pure V at 400 °C. Numbers shown refer to the titanium content of each alloy.

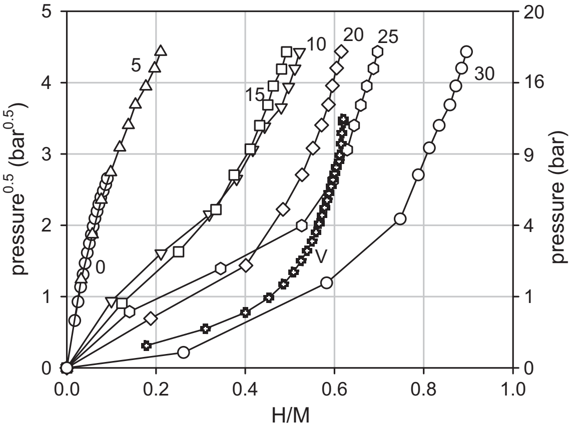

Fig. 5. Hydrogen absorption isotherms for $V_{85-x}Ti_xNi_{15}$ alloys and pure V at 400 °C, presented as a function of the square root of pressure. Numbers shown refer to the titanium content of each alloy.

or H/M. A cubic function has been fitted to each isotherm. There is a clear non-linearity between Ti content and hydrogen absorption.

The absorption isotherm for the $V_{85}Ti_5Ni_{15}$ alloy overlays that of $V_{85}Ni_{15}$, but this can be explained in terms of the bulk composition and volume fraction of the BCC phase. Compared to the $V_{85}Ni_{15}$ base alloy, the BCC phase in the $V_{80}Ti_5Ni_{15}$ alloy has a slightly higher Ti content (4.0 at.%) and slightly reduced Ni content (14.0 at.%), both of which should increase the hydrogen absorption by a small amount. Countering this, the volume fraction of the BCC phase is reduced to 96% by the formation of several compounds with reduced hydrogen absorption.

The decrease in hydrogen absorption for $x = 15$ relative to $x = 10$ can be explained by the decreased BCC volume fraction (84.6% versus 94.7%), and the nearly identical BCC phase composition. Further increases in Ti content result in further increases in hydrogen absorption, which can be correlated with a higher Ti content in the BCC phase, and increasing volume fraction of the $NiTi_2$ phase. Given that attenuating hydrogen absorption is one tool to improve embrittlement resistance, it is of particular interest that the $V_{55}Ti_{30}Ni_{15}$ alloy absorbs significantly more hydrogen than pure V.

Sieverts' law states that the absorption of hydrogen by alloys follows a square root dependency, according to Eq. (1), where C is the hydrogen concentration, k is a constant of proportionality, P is hydrogen pressure and n is the Sieverts' exponent.

$$C = kP^n \tag{1}$$

For ideal systems, n is equal to 0.5, a phenomenon which has its origins in the gas–solid equilibrium between molecular H_2 and dissolved atomic H ($H_{2(g)} \leftrightarrow 2H_{(s)}$). Fig. 5, in which the hydrogen absorption isotherms are presented as a function of $P^{0.5}$, shows that Sieverts' law is obeyed reasonably well over the pressure range of interest for the alloys with the smallest hydrogen absorption (*i.e.*, $x \leq 15$), but as the hydrogen absorption increases, the curves deviate significantly from Sieverts' law by deflecting upwards, indicating that Sieverts' exponent is decreasing). A greater force (*i.e.*, hydrogen partial pressure) is therefore required to drive more hydrogen into the structure as number of available interstices decreases.

Table 1
Chemical and structural characteristics of $V_{85-x}Ti_xNi_{15}$ alloys.

Alloy	Space group	Phase composition (at.%)	Lattice parameter (Å)	Volume fraction (%)
$V_{85}Ni_{15}$	Im3m (229)	$V_{85}Ni_{15}$	3.0093 ± 0.0003	100
$V_{80}Ti_5Ni_{15}$	Im3m (229)	$V_{81.9}Ti_{4.1}Ni_{14.0}$	3.0085 ± 0.0003	96.1
	4_2/mnm (136)	$V_{62.9}Ti_{8.7}Ni_{28.4}$	$a = 8.980$, $b = 4.640$	2.5
	Fd-3m (227)	$V_{28.1}Ti_{42.8}Ni_{29.1}$	3.0150	1.4
$V_{75}Ti_{10}Ni_{15}$	Im3m (229)	$V_{83.4}Ti_{8.8}Ni_{7.8}$	3.0331 ± 0.0003	94.7
	Pm-3m (221)	$V_{12.9}Ti_{45.1}Ni_{42.0}$	3.0150	3.5
	Fd-3m (227)	$V_{15.5}Ti_{30.1}Ni_{54.4}$	11.319	1.8
$V_{70}Ti_{15}Ni_{15}$	Im3m (229)	$V_{83.6}Ti_{8.9}Ni_{7.5}$	3.0350 ± 0.0003	84.6
	Pm-3m (221)	$V_{12.0}Ti_{42.1}Ni_{45.9}$	3.0150	11.7
	Fd-3m (227)	$V_{15.8}Ti_{52.3}Ni_{31.9}$	11.319	3.7
$V_{65}Ti_{20}Ni_{15}$	Im3m (229)	$V_{77.9}Ti_{16.6}Ni_{5.5}$	3.0653 ± 0.0003	87.4
	Pm-3m (221)	$V_{8.5}Ti_{47.4}Ni_{44.1}$	3.0150	7.1
	Fd-3m (227)	$V_{10.3}Ti_{60.1}Ni_{29.6}$	11.319	5.5
$V_{60}Ti_{25}Ni_{15}$	Im3m (229)	$V_{77.2}Ti_{16.3}Ni_{6.5}$	3.0540 ± 0.0003	82.6
	Pm-3m (221)	$V_{8.6}Ti_{47.5}Ni_{43.9}$	3.0150	10.7
	Fd-3m (227)	$V_{12.8}Ti_{57.5}Ni_{29.7}$	11.319	6.7
$V_{55}Ti_{30}Ni_{15}$	Im3m (229)	$V_{63.8}Ti_{29.3}Ni_{6.9}$	3.0998 ± 0.0003	90.3
	Pm-3m (221)	$V_{8.2}Ti_{48.9}Ni_{42.9}$	3.0150	4.4
	Fd-3m (227)	$V_{9.4}Ti_{61.2}Ni_{29.4}$	11.319	5.3

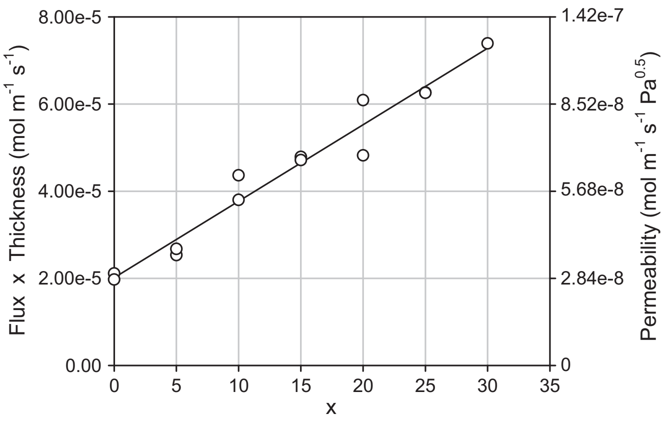

Fig. 6. Hydrogen flux and permeability of $V_{85-x}Ti_xNi_{15}$ alloy membranes at 400 °C.

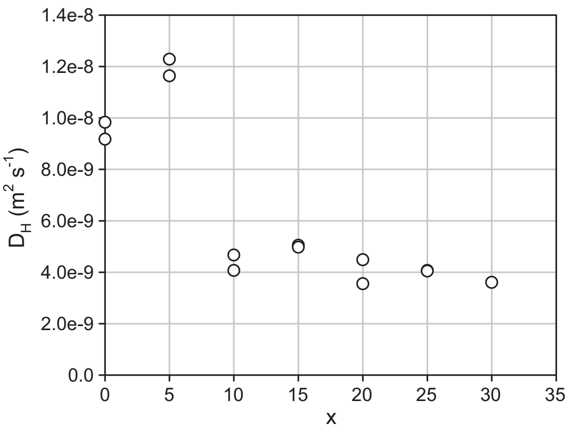

Fig. 7. Calculated diffusion coefficients for atomic hydrogen through $V_{85-x}Ti_xNi_{15}$ alloys at 400 °C.

3.3. Hydrogen permeability

Fig. 6 shows the measured hydrogen flux (*J*), normalised for the inverse of membrane thickness (*z*), for all alloys in the series. All measurements were made at 400 °C with a feed pressure of 6 bar(a). The second *y*-axis shows corresponding permeability values, calculated using the assumption that Sieverts' law is followed as per Eq. (1). The data shows the flux increases monotonically with increasing Ti content. A linear regression of the data results in a relationship ($r^2 = 0.96$) of the following form, where *x* is the Ti content (at.%) in the $V_{85-x}Ti_xNi_{15}$ alloys:

$$Jz = (2.02 \times 10^{-5})x + (1.75 \times 10^{-6})\,\text{mol m}^{-1}\,\text{s}^{-1} \quad (2)$$

An important observation is that the permeability of $V_{55}Ti_{30}Ni_{15}$ (1.05×10^{-7} mol m^{-1} s^{-1} Pa$^{-0.5}$) approaches that of pure V [1]. The permeability of pure V, however, is very difficult to measure due to rapid embrittlement and fracture of the material under test conditions. This illustrates that the $V_{55}Ti_{30}Ni_{15}$ has a significantly more stable structure than V, even with a greater H/M.

3.4. Calculated diffusion coefficients

Bulk diffusion coefficients for hydrogen through the bulk alloy can be calculated via Fick's first law of diffusion [27]:

$$J = -D\left(\frac{dC}{dz}\right) \quad (3)$$

where *J* is the hydrogen flux, *D* the diffusion coefficient of atomic hydrogen through the alloy, and *dC*/*dz* concentration gradient of hydrogen across the membrane. The calculated diffusion coefficients for atomic H are shown in Fig. 7. The data shows a clear correlation between diffusion coefficient and microstructure, with an increase in the volume fraction of non-BCC compounds leading to a large decrease in diffusion coefficient. This indicates that the rate of diffusion of hydrogen through the NiTi and $NiTi_2$ compounds is significantly slower than through the BCC phase, and as a consequence these compounds act as barriers for hydrogen migration and the path tortuosity for hydrogen migration is increased dramatically. In addition, a previous study [8] has shown an inverse relationship between hydrogen absorption and diffusion coefficient, and this phenomenon may also contribute to the small decrease in diffusion coefficient between $x = 10$ and $x = 30$.

4. Discussion

The single greatest barrier to the commercialisation of non-Pd BCC alloy membranes is their high susceptibility to brittle failure, a direct result of the high solubility of hydrogen in these metals and alloys. This problem is exacerbated during thermal cycling under hydrogen, but it can also be prevalent during steady-state permeation. Hydrogen absorption can instigate a number of failure mechanisms, including decohesion from lattice expansion, lattice strain arising from a hydrogen concentration gradient across the membrane, and β-hydride formation. BCC alloy membranes are especially susceptible to failure during thermal cycling under hydrogen, during which hydrogen absorption increases markedly. Failure of these alloys, especially during thermal cycling, would have a catastrophic effect on an industrial-scale membrane installation.

The alloy membranes used in this study were relatively thick, but intentionally so (to enable fundamental aspects of the alloys to be probed). The challenge remains to demonstrate that alloys of this type can be operated reliably at a thickness which will allow the DOE performance targets (especially flux, cost and durability [28]) to be met. That alloy membranes with equivalent or greater hydrogen absorption than pure V could be reliably operated under conditions which would result in the failure of V illustrates that the multi-phase microstructure stabilizes the structure.

The sharp drop in hydrogen diffusion coefficient which accompanies the formation of the Ni–Ti compounds provides an insight into the preferred pathways for hydrogen diffusion. It was shown in Section 1 that the diffusion coefficient of hydrogen through NiTi is significantly slower than through the primary BCC phase. Previous studies linking hydrogen absorption and diffusion suggest that diffusion coefficients decrease with increasing hydrogen absorption. This phenomenon has been observed for both V-based alloys [8] and Pd-based alloys [29]. The dissolution of Ti into the base $V_{85}Ni_{15}$ BCC alloy would therefore be expected to increase the diffusion coefficient of hydrogen though this phase. The large decrease in hydrogen diffusion coefficient observed with Ti > 10 at.% alloys confirms that microstructural effects outweigh the effects of the BCC composition. The Ni–Ti compounds act as barriers to hydrogen diffusion, and for alloys with an interconnected BCC phase, increase the tortuosity of the BCC diffusion path. Combined, these factors significantly decrease the hydrogen diffusion coefficient through the bulk alloy.

Alloys in this series, particularly those with larger Ti contents, exhibited very high hydrogen absorption under the conditions of interest for membrane-based hydrogen separation. This leads to obvious comparisons with hydrogen storage alloys. At 400 °C and 10 bar, the hydrogen absorption of the $V_{55}Ti_{30}Ni_{15}$ alloy (expressed as H/M) was 0.82, which equates to a hydrogen loading of 1.6 wt.%, comparable to the capacities of commercial AB_5-type storage alloys at 25 °C. Further work would be required to explore the hydrogen absorption behaviour at reduced temperature (and in the plateau region), but these materials certainly show promise for hydrogen storage applications as well as separation applications. Ti–V-based alloys have been reported for hydrogen storage applications (for example [30–32]), but typically with a higher Ti/V ratio than the alloys presented here.

The other main issue arising from the high hydrogen absorption is the effect on hydrogen diffusion. Fick's first law of diffusion (Eq. (3)) describes an ideal case where (i) the solute is dilute (*i.e.*, there is no interaction between solute hydrogen atoms), and (ii) the diffusion coefficient is independent of solute concentration. Recent work on the palladium–hydrogen system has shown a clear deviation from the ideal $n = 0.5$ behaviour which can be described in terms of pressure-dependent diffusion coefficients [33,34]. These effects are exaggerated for BCC alloys, particularly under conditions where the alloy can be described as being saturated with hydrogen. Not only does this lead in interactions between solute atoms and competition for interstices, but it also creates a significant lattice parameter gradient in the direction of permeation. While Fick's approach is probably suitable as an indicative tool, there is a need for an in-depth analysis of hydrogen diffusion through saturated BCC alloys. This will be explored in the near future.

5. Conclusions

Alloy membranes of the composition $V_{85-x}Ti_xNi_{15}$, where $0 \leq x \leq 30$ at.%, have been fabricated and characterised. Addition of Ti results in formation of a multi-phase microstructure containing a V-rich BCC solid solution and NiTi and $NiTi_2$ compounds (with partial V substitution). Ti addition increases the permeability, with a maximum permeability at 400 °C of 1.05×10^{-7} mol m^{-1} s^{-1} Pa$^{-0.5}$ being measured for the $V_{55}Ti_{30}Ni_{15}$ alloy. Permeability is controlled largely by the hydrogen absorption of the alloy, while the rate of diffusion of atomic hydrogen through the alloy is slowed by the formation of the multi-phase microstructure. The high-stability of the alloys, despite high hydrogen absorption, indicates the Ni–Ti compounds stabilise the structure during permeation.

Acknowledgements

This research was funded by the CSIRO Advanced Materials Transformational Capability Platform and the CSIRO Coal Technology Portfolio.

References

[1] S.A. Steward, Review of hydrogen isotope permeability through metals, US National Laboratory Report, 1983, UCRL-53441.
[2] M.D. Dolan, Journal of Membrane Science 362 (2010) 12–28.
[3] C. Nishimura, M. Komaki, S. Hwang, M. Amano, Journal of Alloys and Compounds 330–332 (2002) 902–906.
[4] G. Song, M.E. Kellam, D. Liang, M.D. Dolan, Journal of Membrane Science 363 (2010) 309–315.
[5] J.Y. Yang, C. Nishimura, M. Komaki, Journal of Alloys and Compounds 446–447 (2007) 575–578.
[6] Y. Zhang, T. Ozaki, M. Komaki, C. Nishimura, Journal of Membrane Science 224 (2003) 81–91.
[7] M. Amano, M. Komaki, C. Nishimura, Journal of the Less Common Metals 172–174 (1991) 727–731.
[8] M.D. Dolan, G. Song, M.E. Kellam, D. Liang, Journal of Membrane Science 373 (2011) 14–19.
[9] C. Nishimura, T. Ozaki, M. Komaki, Y. Zhang, Journal of Alloys and Compounds 356–357 (2003) 295–299.
[10] S.N. Paglieri, J.R. Wermer, R.E. Buxbaum, M.V. Ciocco, B.H. Howard, B.D. Morreale, Energy Materials: Materials Science and Engineering for Energy Systems 3 (2008) 169–176.
[11] Y. Zhang, T. Ozaki, M. Komaki, C. Nishimura, Scripta Materialia 47 (2002) 601–606.
[12] T.M. Adams, J. Mickalonis, Materials Letters 61 (2007) 817–820.
[13] K. Hashi, K. Ishikawa, T. Matsuda, A. Aoki, Journal of Alloys and Compounds 404–406 (2005) 273–278.
[14] K. Hashi, K. Ishikawa, T. Matsuda, A. Aoki, Journal of Alloys and Compounds 368 (2004) 215–220.
[15] K. Ishikawa, S. Tokui, K. Aoki, Intermetallics 17 (2009) 109–114.
[16] K. Hashi, K. Ishikawa, T. Matsuda, A. Aoki, Journal of Alloys and Compounds 425 (2006) 284–290.
[17] K. Ishikawa, T. Takano, T. Matsuda, A. Aoki, Applied Physics Letters 87 (2005), 061906-061901–061906-061903.
[18] T. Fukuda, T. Kakeshita, H. Houjoh, S. Shiraishi, T. Saburi, Materials Science and Engineering A 273–275 (1999) 166–169.
[19] J.V. Humbeeck, Advanced Engineering Materials 3 (2001) 837–850.
[20] A. Moitra, K.N. Solanki, M.F. Horstemeyer, Computational Materials Science 50 (2011) 820–823.
[21] R. Schmidt, M. Schlereth, H. Wipf, W. Assmus, M. Mullner, Journal of Physics: Condensed Matter 1 (1989) 2473–2482.
[22] H. Wipf, Physica Scripta T94 (2001) 43–51.
[23] D. Driscoll, NETL Test Protocol: Testing of Hydrogen Separation Membranes, National Energy Technology Laboratory, Morgantown, 2008, DOE/NETL-2008/1335.
[24] K.P. Gupta, Journal of Phase Equilibria and Diffusion 26 (2005) 385–389.
[25] K. Otsuka, X. Ren, Progress in Materials Science 50 (2005) 511–678.
[26] O.N. Senkov, D.B. Miracle, Materials Research Bulletin 36 (2001) 2183–2198.
[27] J.W. Crank, The Mathematics of Diffusion , 2nd ed., Clarendon Press, Oxford, 1975.
[28] C.L. Miller, D.C. Cicero, M. Ackiewicz, Hydrogen from Coal Program: Research, Development and Demonstration Plan for the Period 2007 Through 2016 , The United States Department of Energy, National Energy Technology Laboratory, 2007.
[29] G.H. Holleck, Journal of Physical Chemistry 74 (1970) 503–511.
[30] D. Cauceglia, M.D. Hampton, J.K. Lomness, D.K. Slattery, M. Resan, Journal of Alloys and Compounds 417 (2006) 159–163.
[31] B. Massicot, M. Latroche, J.M. Joubert, Journal of Alloys and Compounds 509 (2011) 372–379.
[32] M. Tsukahara, Materials Transactions 52 (2011) 68–72.
[33] A. Caravella, F. Scura, G. Barbieri, E. Drioli, Journal of Physical Chemistry B 118 (2010) 6033–6047.
[34] S. Hara, M. Ishitsuka, H. Suda, M. Mukaida, K. Haraya, Journal of Physical Chemistry B 113 (2009) 9795–9801.